ELECTRONIC STRUCTURE OF MATERIALS CENTRE

NEW APPLICATIONS OF (e,2e) TECHNIQUES

E. Weigold
Presented at XVII International Conference on the Physics of Electronic and Atomic Collisions, Brisbane, July 1991

New Applications of (e,2e) Techniques

E. Weigold

Electronic Structure of Materials Centre, The Flinders University of South Australia, GPO Box 2100, Adelaide 5001, Australia.

Abstract: The flexibility of the (e,2e) technique in obtaining information on both structure and collision dynamics is demonstrated. Examples of structure information are EMS studies of laser excited Na atoms and amorphous carbon films. The role of post-collision effects and correlations is explored by measurements in the autoionising region of helium and in innershell ionisation of argon.

1. INTRODUCTION

The (e,2e) process, in which the momenta of the incident electron and two emitted electrons in an ionizing collision are completely determined, is capable of revealing a rich variety of information. Depending on the kinematics employed, it is possible to investigate in detail either the dynamics of the ionizing collision or to use the reaction to elucidate the structure of the target and the ion. When used for structure determination, high energies and high momentum transfers are normally employed to ensure the clean knockout of a target electron. (e,2e) spectroscopy or electron momentum spectroscopy (EMS) has recently been extensively reviewed by McCarthy and Weigold (1988, 1991).

For most ionizing collisions, however, the kinematics is asymmetric, the two outgoing electrons having very different energies and the momentum transfer to the target is usually small. Such asymmetric collisions have generally been studied using simple targets such as hydrogen (Weigold *et al.* 1979) or helium (e.g. Ehrhardt *et al.* 1969, 1972) whose structure is known or assumed to be known in order to test our understanding of the ionization mechanism. As the momentum transfer approaches zero, the (e,2e) reaction simulates photo-ionization, and this kinematic region has been used to obtain much useful information on partical oscillator strengths and structure information (e.g. Hammett *et al.* 1976).

The (e,2e) reaction has also been used to investigate final state correlation effects between the continuum electrons. This has mainly focussed on post collision interaction effects (PCI) in the ionization of inner shells resulting in the emission of Auger electrons, particularly the ionization of 2p shell of argon (Sewell and Crowe 1982, 1984; Sandner and Völkel 1984; Stefani *et al.* 1986 and Weigold 1990). The

reaction has also been used to study the correlations between resonance and direct ionisation amplitudes in the autoionizing region of helium (Weigold *et al.* 1975, Pochat *et al.* 1982 and Weigold 1990).

In this communication I discuss briefly several (e,2e) studies recently carried out at Flinders University. These include the first measurements of the electron momentum distributions of an atom in an excited target state and of an oriented target, the application of the EMS technique to condensed matter targets, as well as the measurement of correlation effects in the autoionizing region of helium and in the Auger spectrum of argon.

2. NOTATION

The (e,2e) reaction can be written

$$e_0 + A \rightarrow A_f^+ + e_s + e_e, \tag{1}$$

where the subscripts 0,s and e denote the incident scattered and ejected electron. Although the two emitted electrons are indistinguishable, it is often convenient to call the fast outgoing electron the scattered one and the other the ejected one. Conservation of energy and momentum requires

$$\epsilon_f = E_0 - E_s - E_e, \text{and} \qquad \mathbf{k}_0 = \mathbf{k}_s + \mathbf{k}_e - \mathbf{q}, \tag{2}$$

where ϵ, the separation energy of the electron, is equal to the energy difference between the initial target state A and final state $\mid f >$ of the ion, and $-\mathbf{q}$ is the ion recoil momentum of the ion. In the plane wave impulse approximation $\mathbf{q}$ is the momentum of the struck target electron. The ion recoil energy has been neglected. The momentum transfer to the target is given by

$$\mathbf{K} = \mathbf{k}_0 - \mathbf{k}_s. \tag{3}$$

In noncoplanar and coplanar symmetric (e,2e) experiments K is maximised by choosing $k_e = k_s$ and $\theta_e = \theta_s$.

At high enough energies and momentum transfer the (e,2e) differential cross section is given by

$$\sigma(e,2e) = C f_{ee} \sum_{av} |< f \mid a(\mathbf{q}) \mid i >|^2, \tag{4}$$

where $\sum_{av}$ denotes the usual sum and average over final and initial degeneracies, C contains kinematical factors and f_{ee} is the half-off-shell Mott scattering cross section. In the noncoplanar symmetric geometry f_{ee} is essentially constant and the cross section is simply proportional to the square of the target-ion overlap

amplitude resulting from the annihilation of an electron of momentum $\mathbf{q}$ in the target state $| i >$. This is the EMS region of the (e,2e) reaction.

The weak-coupling expansion of the target ion overlap is

$$< f \mid a(\mathbf{q}) \mid i >= \sum_{\ell} < f \mid \ell >< \ell \mid a(\mathbf{q}) \mid i >, \tag{5}$$

where the orthonormal basis states $| \ell >$ are linear combinations of configurations formed by annihilating one electron in a target ion state. Generally only a single hole state $| j >$ contributes to the expansion in (6). We can define an experimental orbital $\psi_j(\mathbf{q})$ and the spectroscopic factor $S_f^{(j)}$ by

$$\psi_j(\mathbf{q}) \equiv < j \mid a(\mathbf{q}) \mid i > \quad \text{and} \quad S_f^{(j)} = |< f \mid j >|^2 \tag{6}$$

3. ELECTRON MOMENTUM SPECTROSCOPY OF LASER EXCITED ATOMS

Excited target atoms can be prepared in well defined states by optically pumping atoms with a tuneable laser. By using polarised laser light it is possible to excite specific magnetic substates. This offers the possibility of measuring momentum distributions for excited targets as well as for atoms in aligned and oriented states. In the recent measurements of Zheng *et al.* (1990) and Bell *et al.* (1991a) sodium atoms are optically pumped by right hand circularly polarized laser light tuned to the $3^2S_{1/2}(F=2) \leftrightarrow 3^2P_{3/2}(F' = 3)$ transition. The excited pumped atoms are in the $m_{F'} = 3$ state, or in terms of orbital momentum in the $m_\ell = +1$ state.

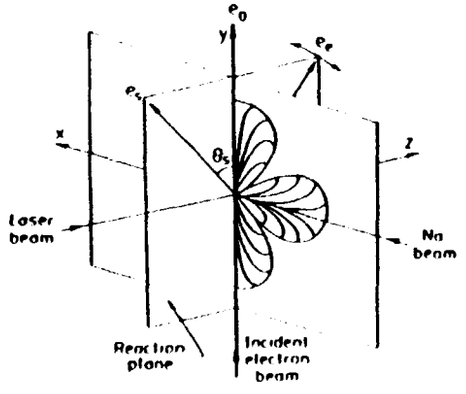

Fig.1 Schematic diagram of the experimental arrangement and the 3p($m_\ell = 1$) electron densities.

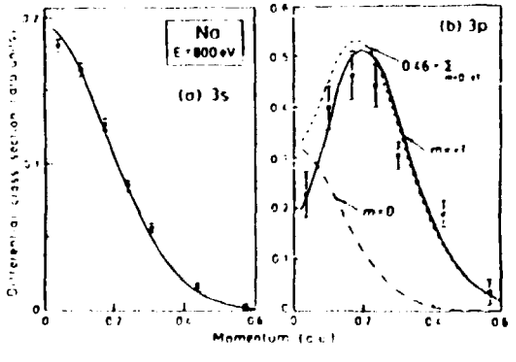

Fig.2 The momentum distributions for (a) the 3s ground state and (b) 3p excited state of Na compared with HF momentum distributions

The kinematics is shown in fig. 1, which also shows schematically the $3p_x$ and $3p_y$ electron density distribution of the excited sodium. The scattering plane is the zy plane and $\theta_s = \theta_e = 45°$, the azimuthal angle ϕ of the ejected electron is varied to probe the different momentum components of the target. Thus the experiment measures the (e,2e) triple differential cross section as a function of the x component of momentum, q_x. The z and y components of momenta are fixed and essentially zero for small binding energies. Due to the finite resolution of the spectrometer, the average values of q_y and q_z are not quite zero, being of the order of 0.06 a.u.

The momentum distributions obtained for the 3s ground state transition and for the $3p(m_\ell = 1)$ excited state are shown in figs. 2(a) and (b) respectively compared with calculated momentum distributions given by the Hartree-Fock 3s and 3p wavefunctions. The finite momentum resolution has been included in the calculations, its main effect is to fill in the 3p momentum distributions at momenta close to zero. The momentum distribution for the excited state peaks at very small momenta (~ 0.2 a.u.) because of the diffuse nature of the 3p orbital in coordinate space.

4. THE SPECTRAL MOMENTUM DENSITY OF AMORPHOUS CARBON

The (e,2e) technique can be used to obtain the spectral momentum density of electrons in solids, that is the probability of an electron possessing a particular value of binding energy ϵ and momentum $\mathbf{q}$. Ritter, Dennison and Jones (1984) reported the first spectral momentum density measurement of the valence band of a solid, the target material in this case being an amorphous carbon film. With an (e,2e) energy resolution of approximately 6eV, they were barely able to resolve two bands in the binding energy spectrum.

There has been considerable interest in determining the electronic properties of amorphous carbon (see Gao *et al.* 1989 and references therein). Amorphous carbon (a-C) films range from black, soft "graphite" films to hard, transparent "diamond-like" films depending on the method of preparation and the concentration of hydrogen in the sample (Ritter *et al.* 1984). The structure of a-C films is still not understood.

In order to obtain further information on the electronic structure of a-C, we have undertaken a series of (e,2e) measurements on evaporated films of a-C at much higher energy resolution than the above earlier work. In the present work a primary electron beam of 10keV plus binding energy intersects a free-standing 80Å amorphous carbon film. Scattered electrons leaving the collision region at angles of 45 degrees with respect to the incident beam direction pass through two identical hemispherical electrostatic analysers positioned on opposite sides of the beam. The analysers are used to determine the momenta and arrival times of each emitted electron by means of position sensitive detectors (Lower and Weigold 1989). Each analyser is adjusted to accept electrons in a 20eV band of energies centred around 5000eV. The combined energy resolution of each analyser and detector together is

about 1eV. Different values of momenta q perpendicular to the incident direction and in the scattering plane are sampled by varying $\Delta E = E_s - E_e$ keeping $E_s + E_e = E_0 - \epsilon(\mathbf{q})$ constant. The values of q are given by

$$q = k_0 \frac{\Delta E}{2E_0}\left(1 + \frac{\epsilon}{E_0}\right) \tag{7}$$

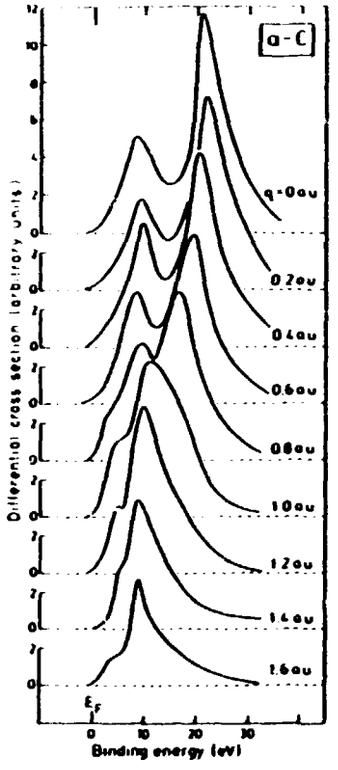

Fig.3 Spectral momentum density spectra for amorphous carbon (Lower *et al.* 1991).

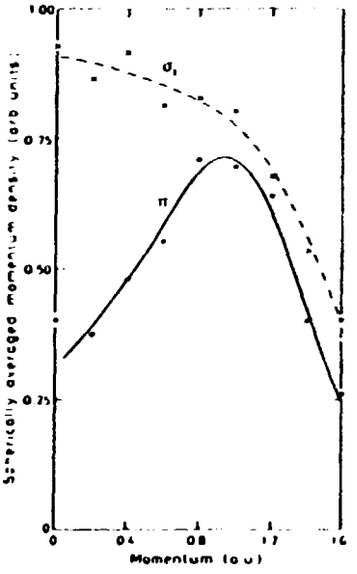

Fig.4 Momentum densities for the valence π and σ bands of a-C (Lower *et al.* 1991).

Fig. 3 shows binding energy spectra obtained at different target electron momenta (Lower *et al.* 1991). This is a plot of the spectral momentum density. The low energy peak is attributed to the excitation of a graphitic π-band and the higher energy peak to the excitation of graphitic σ-bands. The data has been deconvoluted to allow for the effects of energy loss by incident and scattered electrons within the target material due to multiple scattering. The strongly dispersive nature of the higher energy σ band can be seen from the figure. The outer π band also shows some dispersion. In addition to the dispersion, there is for both bands a marked change in intensity as a function of q. This is displayed in fig. 4, which shows the momentum density as a function of q for the two bands.

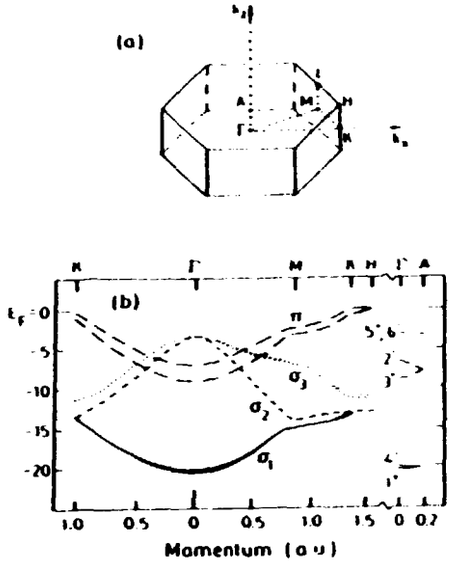

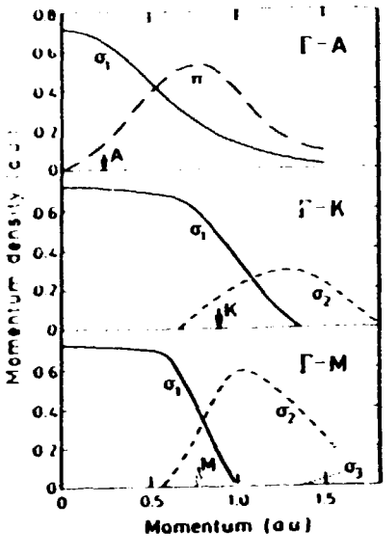

Fig.5 Brillouin zone and valence band structure of graphite (Goa *et al.* 1988).

Fig.6 Calculated spectral momentum densities for the valence bands of graphite in the different crystal directions

The band structure of graphite as calculated by Gao *et al.* 1988 is shown in fig. 5, and the momentum densities for the π and three σ bands in fig. 6. The lowest σ band is σ_1 and its wavefunction is s-like, i.e. the momentum density is maximum at $q = 0$ and decreases monotonically as q increases. The wavefunctions for the upper two σ bands are p-like, the momentum density being zero at $q = 0$, and rising abruptly from zero near the Brillouin zone boundary to peak in the second and third zones, and then falling as q increases. Thus the σ_2 and σ_3 bands are essentially unoccupied at small q (≤ 0.5 a.u.). The momentum density for the π band is zero for **q** in the $\Gamma - K - M$ plane, since the π orbital has a node there. For **q** along the C axis perpendicular to the basal plane the momentum density of the π band displays p-wave character, it is zero at the origin and peaks at $q \approx 0.7$ a.u. In the present work we expect random orientations in the disordered phase of the evaporated films. This would still preserve the p-wave and s-wave character of the π and σ_1 bands, respectively.

Fig. 4 shows that the σ_1 band does indeed have s-wave character, having greatest momentum density at smaller q. The momentum density for the lower-energy π band does increase somewhat with q, as expected from the predicted p-wave character. There is some evidence that for diamond-like structures the momentum density for the outer-valence band does not go to zero (Gao *et al.* 1989). The spectral density for the π band is rather larger than expected for graphite. The

data are therefore not consistent with the film being completely graphitic.

5. CORRELATIONS IN INNER-SHELL IONISATION : AUGER PROCESSES IN ARGON

The (e,2e) technique has been applied to study the ionisation of the 2p core level of argon by a number of groups. These experiments, proposed by Berezhko *et al.* (1978), detect the decay Auger electron in coincidence with the scattered electron, thus selecting momentum transfer and energy loss. The reaction can be written as

$$\begin{aligned} e^- + Ar \rightarrow & Ar^+(J,M) + e_s^- + e_e^- \\ & \downarrow \\ & Ar^{2+}(J',M') + e_A^-. \end{aligned} \tag{8}$$

Sewell and Crowe (1982,1984), Stefani *et al* (1986) and Sandner and Völkel (1984) measured angular correlations between the Auger and scattered electrons for the $L_3M_{23}M_{23}(^1S_0)$ transition. Sandner and Völkel (1984) and Stefani *et al.* (1986) observed post collision interaction (PCI) effects close to threshold, the slow ejected electron transferring energy to the decay Auger electron. These experiments were all based on single parameter detection techniques, and the measurements could only be carried out by using very large energy windows on the scattered electron detector with a corresponding large spread in the energy of the near threshold ejected electron. In the present experiments we use a multiparameter coincidence spectrometer to examine simultaneously with improved energy resolution the whole argon Auger spectrum in the region 200-208eV in coincidence with scattered electrons as a function of the energy and angle of emission of the Auger electrons at several incident energies close to threshold. The spread in energy of the scattered and ejected electrons was only 3eV in these measurements, compared with about 10eV in previous measurements.

In the large distance eikonal approximation (Kuchiev and Sheinerman 1989), the energy shift ΔE_A in the Auger electron spectrum is given by

$$\Delta E_A = -\frac{\xi\Gamma}{2}, \tag{9}$$

where Γ is the width of the intermediate state and

$$\xi = \frac{1}{v_{sA}} - \frac{1}{v_s} + \frac{1}{v_{Ae}} - \frac{1}{v_e}. \tag{10}$$

In all measurements $v_e << v_s, v_A$ and $\xi \sim -1/v_e$. Thus the shift in energy $\Delta E_A = \Gamma/2v_e$ is positive and decreases as $E_e^{-1/2}$. For $v_e \sim v_S \sim v_A$ the post collision effects are a strong function of the angle of emission of the three electrons.

Fig. 7 shows a coincidence and noncoincidence Auger spectrum taken at just above threshold (Bell *et al.* 1991b). The coincidence spectrum shows an observable shift to higher energy, showing the significance of post collision interactions. The shift as a function of energy above threshold is shown in fig. 8 for the $L_3M_{23}M_{23}(^1D_2)$ transition compared with $\Delta E = \Gamma/2v_e$. The shape of the Auger line also depends sensitively on the parameter ξ (Kuchiev and Sheinerman 1989).

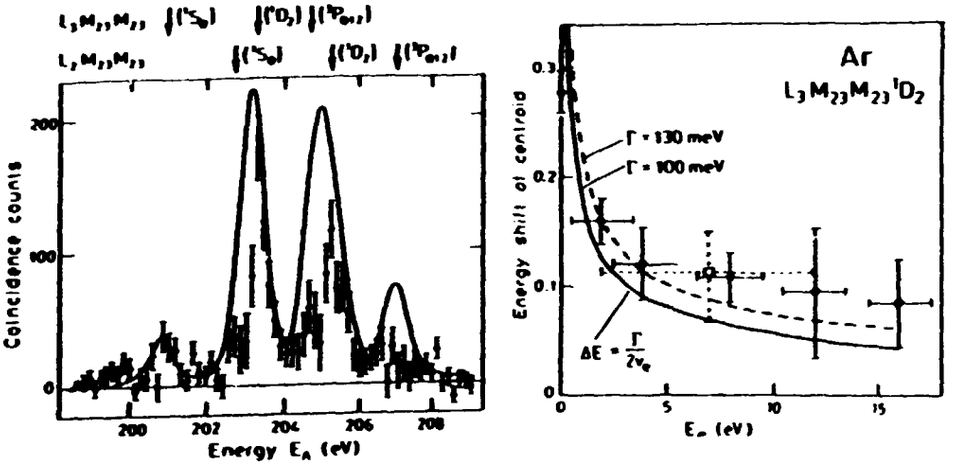

Fig.7 Coincidence spectra and non coincidence spectra (solid line) taken simultaneously with E_0 = 750eV, E_e = 496eV, $\theta_A = 135°$, $\theta_e = -18°$.

Fig.8 The PCI shift ΔE_A of Auger peak centroids as a function of E_e compared with eq.9 for the $L_3M_{23}M_{23}{}^1D_2$ transition (•). The square is the data point of Stefani *et al.* (1986).

Berezhko *et al.* (1978) showed in the two-step plane-wave Born approximation that the probability of Auger electron emission in the scattering plane is given by

$$I(\theta_A)\alpha 1 + \beta\cos 2(\theta_A - \psi), \tag{11}$$

where the anisotropy parameter β and the angle ψ are related to alignment and statistical tensors. In the Born approximation $\psi = \theta_K$, the direction of momentum transfer. Thus angular correlations can lead to the determination of electron correlation effects.

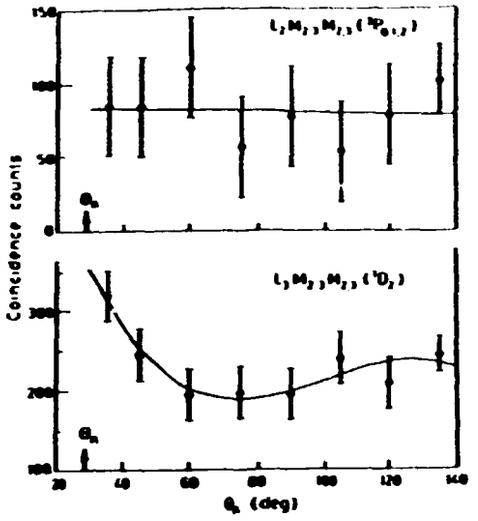

Fig.9 Angular correlations for argon Auger electrons in coincidence with scattered electrons E_e = 496eV, θ_e = -16°, E_0 = 753eV.

Fig. 9(a) and (b) show respectively the angular correlations observed by Bell *et al.* (1991c) for the $L_2M_{23}M_{23}(^3P)$ and $L_3M_{23}M_{23}(^1D_2)$ transitions. The former must be isotropic since $J = \frac{1}{2}$ for the $2p_{\frac{1}{2}}$ shell and the initial state cannot be aligned.

6. (e,2e) COINCIDENCE MEASUREMENTS IN THE AUTOIONISING REGION OF HELIUM

The autoionisation of atoms by electron impact involves in general the interference between the direct and the resonance ionisation amplitudes. This interference depends on the momenta of the scattered and ejected electrons and on the momentum transfer . Therefore (e,2e) cross section measurements in the autoionising region can provide very sensitive information on details of the excitation process of the resonance as well as on the interference of the resonance process with direct ionization.

Tweed (1976) showed that the triple differential (e,2e) cross section in the vicinity of the rth autoionising resonance can quite generally be written in the parameterized form originally due to Shore (1967),

$$\frac{d^3\sigma}{d\Omega_e d\Omega_e dE_e} = f(\mathbf{k}_e, \mathbf{K}) + \sum_\mu \frac{a_\mu(\mathbf{k}_{e\mu}, \mathbf{K}_\mu)\epsilon_\mu + b_\mu(\mathbf{k}_{e\mu}, \mathbf{K}_\mu)}{1 + \epsilon_\mu^2}, \tag{12}$$

$$\text{where } \epsilon_\mu = 2(E_e - \dot{E}_\mu)\Gamma_\mu^{-1}, \tag{13}$$

and $\dot{E}_\mu$ and E_e are respectively the energies of the rth autoionising resonance and the energy of the ion plus continuum emitted electron (relative to the energy of the residual ion) with total angular momentum and spin quantum numbers denoted by

$\mu = \{\nu; L, M, S\}$. f is simply the cross section for direct ionization, a_μ is a measure of the asymmetry of the resonance profile and b_μ of its contributions to the cross section.

Fig. (10) provides some examples of the observed coincidence ejected electron spectra (Lower and Weigold 1990). We see a series of resonance profiles superimposed upon a background of direct ionization events. The final fitted function is represented by the solid curve, whilst the fitted direct ionization background f and the individual fitted resonance profiles $(a\epsilon + b)/(\epsilon^2 + 1)$ convoluted with the instrumental response, are indicated by dashed lines. Both spectra were obtained in the binary region with the only difference being 18° in the angle of the ejected electron. This is a clear demonstration of how sensitive the cross sections are to the ejected electron momentum.

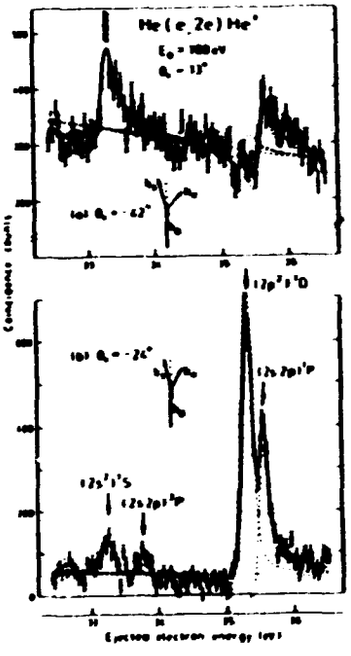

Fig.10 Coincidence ejected electron spectra for $He(e,2e)He^+$.

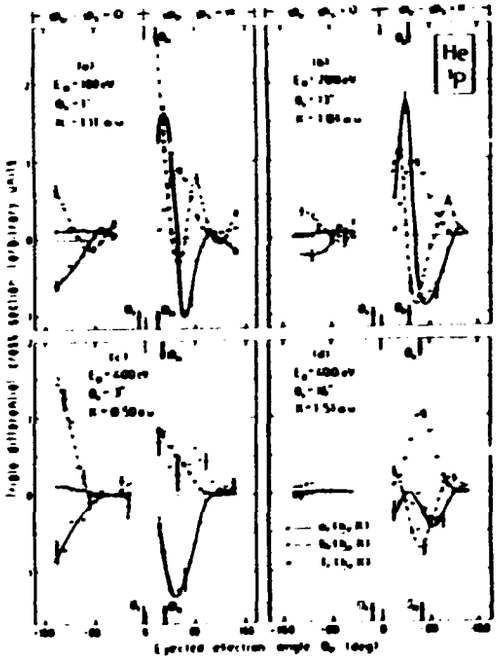

Fig.11 The direct (e,2e) cross section f and parameters a_ν and b_ν for the $(2s2p)^1P$ resonance in He (Lower and Weigold 1990).

Values for a_ν, b_ν and f_ν deduced from the fitting of individual ejected electron spectra for the $(2s^2)^1S$, $(2s2p)^1P$ and $(2p^2)^1D$ resonances show rapid variations as a function of θ_e. Fig. 11 shows the results for the $(2s2p)^1P$ state for four different combinations of incident energies and scattering angles. Since absolute cross sections were not obtained the results have been normalized to the maximum value of f under the $(2s^2)^1S$ resonance profile at each particular energy and scattering angle, and this maximum has been set to 1 unity. The direct ionization cross section f for

each incident energy and scattered electron angle appears in essentially two lobes. The major lobe (the binary lobe) occurs approximately in the momentum transfer direction. The second occurs roughly 180° away and can be associated with recoil collisions involving momentum transfer to the residual ion. For each resonance and at each energy and scattering angle, the a_r and b_r parameters show smooth oscillation between positive and negative values as the ejection angle varies. Positive values of b_r correspond to constructive interference between direct and resonant ionization amplitudes, resulting in localized increases in the (e,2e) cross section. Negative values of b_r are related to a decrease in the cross section due to the effects of destructive interference. Positive values of a_r correspond to a profile showing a minimum followed by a maximum in the sense of increasing ejection energy, whilst the reverse occurs when a_r is negative.

The results for all three resonances show strong interference, both constructive and destructive, between the direct and resonance amplitudes. The resonance parameters show even more rapid variation in magnitude as a function of the ejected electron angles than does the direct cross section. Although the peak structures in a_r and b_r are correlated with the direction of the momentum transfer θ_K, as is that for the direct cross section f_r, the correlation is not simple. Considerable amount of theoretical effort is needed to explain the data. First order theories are inadequate since they would give the K direction as a symmetry axis, which is clearly in violation of the measurements.

7. SUMMARY

The richness of information that can be obtained by the application of the (e,2e) technique has been demonstrated by discussing four different types of experiments. Two examples involve the determination of structure information in kinematic regions where the (e,2e) collision process is well understood. The other two examples involve the determination of subtle effects in the collision dynamics.

ACKNOWLEDGEMENTS

I am grateful to the ARC for financial support of this work and would like to acknowledge the essential role played by the other members of the Flinders (e,2e) group.

References

Bell S, Shen Y, Weigold E and Zheng Y 1991a Proc. 17th ICPEAC p177
Bell S, Hall D, Samardzic O and Weigold E 1991b Proc. 17th ICPEAC p200
Bell S, Shen Y, Weigold E and Zheng Y 1991c Proc. 17th ICPEAC p201
Berezhko E G, Kabachnik N M and Sizov V V 1978 J Phys B: At Mol Phys 11 1819
Ehrhardt H, Hesselbacher K H, Jung K, Schultz M, and Willmann K 1972 J Phys B At Mol Phys 5 2107
Ehrhardt H, Schultz M, Tekaat T and Willmann K 1969 Phys Rev Lett 22 89
Gao C, Ritter A L, Dennison J R and Holzworth N A W 1988 Phys Rev B 37 3914

Gao C, Wang Y Y, Ritter A L and Dennison J R 1989 Phys Rev Lett **62** 165
Hamnett A, Stoll W, Branton G, Brion C E and van der Wiel M J 1976 J Phys B: At Mol Phys **9** 945
Kuchiev M Yu and Sheinerman S A 1989 Sov Phys Usp **32** 569
Lower J and Weigold E 1989 J Phys E:Sci Instrum **22** 421
Lower J and Weigold E 1990 J Phys B **23** 2819
Lower J, Bharathi S M, Chen Y, Nygaard K J and Weigold E 1990 (to be published)
McCarthy I E and Weigold E 1988 Rep Prog Phys **51** 299
McCarthy I E and Weigold E 1991 Rep Prog Phys **54** (June issue)
Ritter A L, Dennison J R and Jones R 1984 Phys Rev Lett **53** 2054
Sandner W and Völkel M 1984 J Phys B: At Mol Phys **17** L597
Sewell E C and Crowe A 1982 J Phys B: At Mol Phys **15** L357
Sewell E C and Crowe A 1984 J Phys B: At Mol Phys **17** 2913
Shore B W 1967 J Opt Soc Am **57** 881
Stefani G, Avaldi L, Lahmam-Bennani and Duguet A 1986 J Phys B **19** 3787
Tweed R J 1976 J Phys B **9** 1725
Weigold E, Noble C J Hood S T and Fuss I 1979 J Phys B: At Mol Phys **12** 291
Weigold E 1990 Aust J Phys **44** 277
Weigold E, Ugbabe A and Teubner P J O 1975 Phys Rev Lett **35** 209
Zheng Y, McCarthy I E, Weigold E and Zhang D 1990 Phys Rev Lett **64** 1358